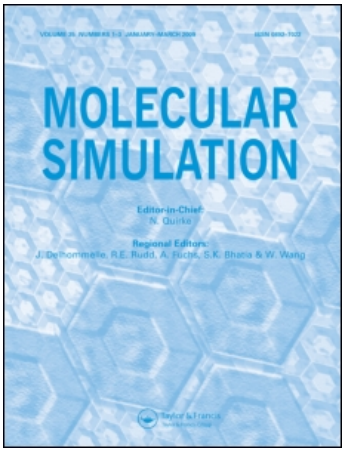

Molecular Simulation
Publication details, including instructions for authors and subscription information:
http://www.informaworld.com/smpp/title~content=t713644482

Some Recent Developments in Computational Chemistry

N. Quirke[a]
[a] European Centre for Computational Science and Technology, Biosym, Parc Club Orsay Université, Orsay Cedex, France

To cite this Article Quirke, N.(1996) 'Some Recent Developments in Computational Chemistry', Molecular Simulation, 16: 1, 193 — 208
To link to this Article: DOI: 10.1080/08927029608024072
URL: http://dx.doi.org/10.1080/08927029608024072

Molecular Simulation, 1996, Vol. 16, pp. 193–208
Reprints available directly from the publisher
Photocopying permitted by license only

SOME RECENT DEVELOPMENTS IN COMPUTATIONAL CHEMISTRY

N. QUIRKE[+]

European Centre for Computational Science and Technology, Biosym, Parc Club Orsay Université, 20, rue Jean Rostand, 91893 Orsay Cedex, France

(Received March 1995, accepted March 1995)

Some recent developments in the use of computational methods to predict the properties of condensed phases are discussed; the use of Gibbs ensemble Monte Carlo to predict the phase equilibria of bulk phases, the use of molecular dynamics to elucidate Atomic Force Microscopy experiments on organic films, and the use of combined Monte Carlo/molecular dynamics techniques to enable the direct prediction of particle fluxes along pressure gradients in model microporous materials.

KEY WORDS: Gibbs ensemble, atomic force microscopy, grand canonical molecular dynamics, particle flux, micropores.

1 INTRODUCTION

The last fifteen years have seen a dramatic expansion of the use of molecular simulation techniques to study condensed phase properties. The focus of activity has moved away from the study of the bulk phase behaviour and transport properties of 'simple' model atomic systems such as Lennard-Jones fluids towards more realistic molecular models, more accurate predictions of physical properties and towards more 'complex' problems. For example, molecular simulation is now used routinely to elucidate the molecular origins of biological activity, or the nature of collective and individual behaviour of molecules at surfaces or in confined geometries. These changes have been driven by advances in computer hardware (the increasing accessibility of fast workstations), improvements in methodology (both the availability and accuracy of forcefields for organic and inorganic molecules and the development of new methods such as the Gibbs ensemble) and by the needs of industries in the pharmaceutical and chemical sectors to cut costs by introducing modelling of complex problems at an early state in product development.

The aim of the present article is to reflect a little of this diverse activity by discussing some results in three areas where recent progress has been encouraging and which open up some new possibilities for the future: 1) The prediction of accurate phase diagrams for molecular fluids 2) The use of molecular dynamics to mimic and extend analytical techniques, in particular Atomic Force Microscopy of organic interfaces and 3) The direct prediction of transport properties of adsorbents using novel combinations of Monte Carlo and molecular dynamics simulation.

[+]Address for correspondence: Dept. of Chemistry, University of Wales at Bangor, Gwynedd LL57 2UW, UK.

2 PREDICTION OF PHASE EQUILIBRIA

Molecular simulation has been used for some time to predict the properties of liquids. However, recently new algorithms and approaches have been developed, especially within the Monte Carlo scheme which allow the direct prediction of phase equilibria, rather than its derivation from simulation data (*e.g.* chemical potentials) calculated in each candidate phase (1). In particular the Gibbs ensemble algorithm (2, 3) will *predict* the coexisting phases of a model fluid; a prior knowledge of the phase boundaries is not required. In the Gibbs ensemble two (or more) Monte Carlo simulations are linked so as to force them to be in equilibrium. In a two-phase region the algorithm ensures that one of the simulations predicts the properties of (say) the vapour phase and the other the coexisting liquid phase. Similarly in a region of liquid-liquid equilibrium the simulation will predict the properties of the coexisting liquid phases. It is not necessary to know the coexisting pressures or chemical potentials, these are predictions of the method. In a single-phase region the two simulations predict the same single phase. Three types of trial displacements are made in the Gibbs simulation to generate new configurations corresponding to equilibrium phases; they are illustrated below:

Box 1: N_1, V_1, T Box 2: N_2, V_2, T

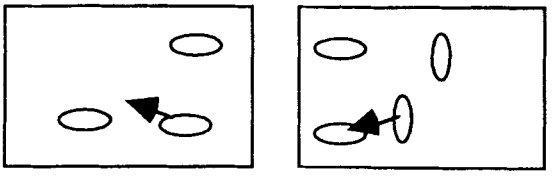

Move

$$P_{move} = \min[1, \exp(-\beta\Delta U_1 - \beta\Delta U_2)]$$

Figure 1a Trial moves in each simulation box (each within PBC). The term $\beta\Delta U$ represents the energy change of the configuration on the displacement of a molecule, $\beta = 1/k_bT$. The molecular moves in each box may also be considered independently.

Box 1: $N_1, V_1 + \Delta V, T$ Box 2: $N_2, V_2 - \Delta V, T$

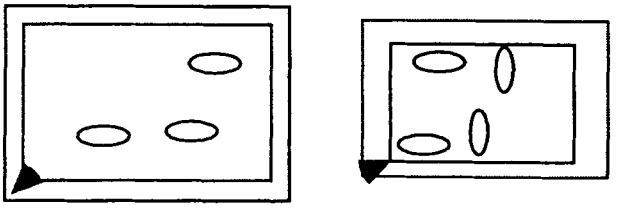

Volume

$$P_{\text{Volume}} = \min[1, \exp(-\beta\Delta U_1 - \beta\Delta U_2 + N_1 \ln((V_1 + \Delta V)/V_1) + N_2 \ln((V_2 - \Delta V)/V_2))]$$

Figure 1b Trial volume exchange between boxes.

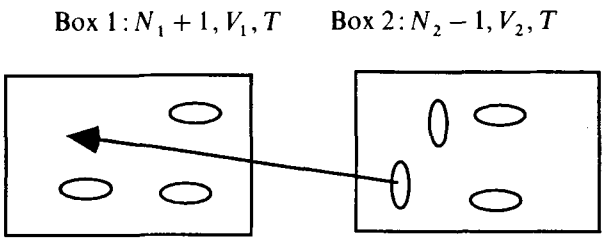

Transfer

$$P_{\text{transfer}} = \min [1, \exp (-\beta\Delta U_1 - \beta\Delta U_2 - \ln((N_1 + 1)\, V_2/(N_2\, V_1)))]$$

Figure 1c Trial transfer of a molecule.

These trial moves are accepted with a probability proportional to P_{Trial} and ensure that the Gibbs conditions for thermodynamic equilibrium ($P_1 = P_2$, $T_1 = T_2$, $\mu_1 = \mu_2$, where μ is the chemical potential) are obeyed. Modifications of the algorithm allow Gibbs simulations of mixtures at constant pressure or phase equilibria in the presence of external fields (3). As an example of the power of this technique the next section presents results for the fluid phase properties of ethane.

2.1 Fluid Phase Equilibria of Ethane

Figures 2a and 2b show the accuracy with which the liquid-vapour coexistence and high pressure properties of ethane can be predicted using the simplest possible effective

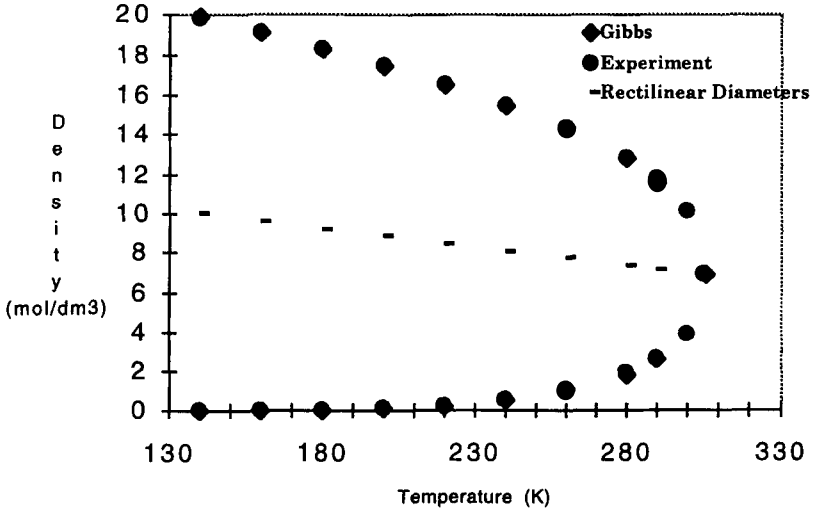

Figure 2a Liquid-vapour coexistence region for ethane as predicted using the Gibbs ensemble Monte Carlo method. The experimental data is from reference 8: where only one symbol can be seen, the Gibbs data is underneath.

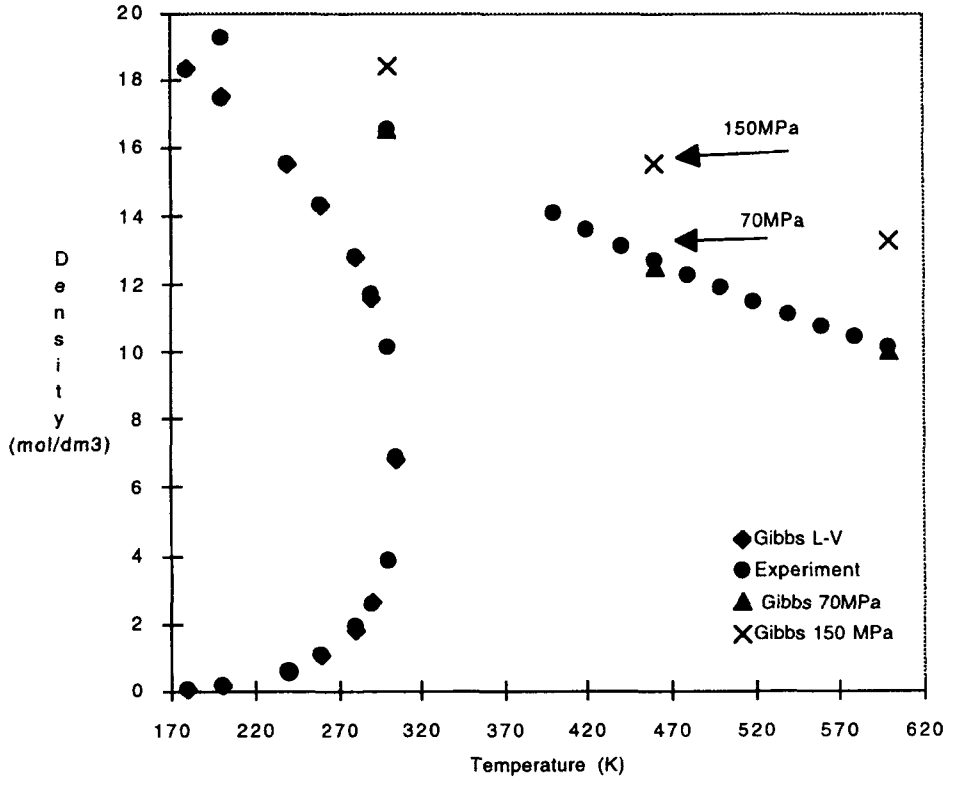

Figure 2b High pressure isobars for ethane predicted using constant pressure (Gibbs ensemble) Monte Carlo. The solid circles show experimental data (8) and the diamonds, triangles and crosses are the predictions of Gibbs ensemble simulation. The experimental data in reference 8 do not go above 70 MPa, molecular simulation data has been obtained for pressures of 150 MPa and 1000 MPa (not shown).

molecular potential function, a two-centre Lennard-Jones potential with the Gibbs ensemble. The effective potential was obtained by fitting the experimental saturated densities and pressure at one temperature (260 K) to within the statistical error (see entry in Table 2). The new potential parameters differ by a few percent from most previous effective 2cLJ's potentials (Table 1). This is enough to produce a dramatic improvement in the accuracy of the phase properties.

The fitted potential was then used to *predict* the remaining fluid coexistence curve. The results of using Gibbs ensemble Monte Carlo simulations over the subcritical range are shown in Table 2 and Figure 2a. The simulations were carried out with 108 molecules in each simulation with a cut off radius equal to half the box size and full long range corrections. The averages were taken over ~ 10 million configurations at high temperatures to ~ 40 million at low temperatures with about half that amount for equilibration. The statistical errors were obtained by calculating the statistical correlation length (7) in the data and are quoted at one standard deviation. The fluctuations are larger at higher temperature than low although the error reported also depends on the length of the simulation at a given temperature. Above $T = 180$ K differences between simulation and experiment are within the statistical error, below $T = 180$ K the

Table 1 Effective potentials for Two centre Lennard-Jones models of ethane. In this work the potential was cut (but not shifted) at half the box length and a long range correction applied. This correction was obtained by performing a numerical integration over the angular degrees of freedom as well as the pair separation out to 20σ after which the bond length was set to zero. The resulting long range correction can differ by (say) 10%from a correction based on setting the bond length to zero outside the cut off.

Sigma (Å)	*Epsilon (K)*	*Bond Length l (Å)*	*Bond Length (/ σ)*	*Reference*
3.775	104.165	1.53	0.405	4
3.506	137.5	2.345	0.669	5
3.520	137.5	2.345	0.666	1
3.512	139.81	2.353	0.670	6
3.4956	135.0	2.353	0.673	This work

Table 2 Coexistence region data for ethane. The data in brackets are the experimental data from reference 8.

T (K)	*Liquid density mol/dm³*	*Vapour density mol/dm³*	*Liquid pressure MPa*	*Vapour pressure MPa*
290	11.60 (11.73)	2.62 (2.599)	3.85 (3.515)	3.518 (3.515)
280	12.77 (12.77)	1.82 (1.898)	0.94 (2.806)	2.96 (2.806)
260	14.33 ± .05 (14.31)	1.09 ± .05 (1.06)	1.92 ± 1.02 (1.72)	1.66 ± .07 (1.72)
240	15.51 ± .03 (15.51)	0.60 ± .1 (0.59)	1.08 ± .22 (0.97)	1.01 ± .06 (0.97)
220	16.54 (16.54)	0.30 (0.3025)	2.25 (0.4923)	0.49 (0.4923)
200	17.51 (17.45)	0.135 (0.1399)	0.41 (0.2174)	0.203 (0.2174)
180	18.36 ± .006 (18.30)	0.055 ± .012 (0.05456)	0.11 ± .19 (0.07874)	0.081 ± .007 (0.07874)
160	19.11 (19.09)	0.015 (0.0164)	0.18 (0.02146)	0.021 (0.02146)
140	19.95 (19.86)	0.0031 (0.00332)	1.6 (0.00383)	0.0035 (0.00383)

differences are outside the error. The average absolute deviations from experiment were 0.2%for the liquid density, 3%for the vapor density and 3%for the vapor pressure (the statistical uncertainties are greatest in the liquid pressure, consequently the vapour pressure is used as the best estimate of the saturated pressure).

The critical temperature and pressure may be estimated by obtaining the best fit for the simulation data to the relations,

$$0.5\,(\rho_l - \rho_v) = B_1 |\delta T|^{0.32}$$
$$0.5(\rho_l + \rho_v) = \rho_c + B_2 |\delta T| \qquad (1)$$

Taking the range, $T = 200$ to 290 K, the estimated critical temperature for ethane is 305.7 K (experiment 305.34 K) and the estimated critical density is 6.82 mol/dm^3 (experiment 6.88 mol/dm^3). Minor variations of less than one percent could be observed by varying the temperature range for the fit.

Sadus and Prausnitz [28] have found significant differences between the vapour-liquid coexistence curves in the critical region for effective argon potentials based on 2-body and a combination of 2 and 3 body terms. Away from the immediate critical region however the 3-body repulsive and attractive terms cancel and the coexistence curves are similar. In employing equation 1 outside of the immediate critical region possible errors due to the lack of 3-body contributions may be avoided (as may computational errors due to finite size effects in the Gibbs simulations).

It is of interest to see if the effective potential is also accurate over a much wider range of conditions than the coexistence region. Accordingly in Figure 2b the high pressure isobar (70 Mpa) has been predicted using isothermal-isobaric (NPT) Monte Carlo simulation. The agreement with experiment is excellent as can be seen in Table 3 and Figure 2b. Note that results quoted are for 32 molecules; comparison with results for 108 molecules at similar state points showed that the two system sizes agreed to within the combined statistical error ($\sim$ 1% in the densities).

Given that the effective potential is able to reproduce the known fluid phase diagram to within the statistical error it is reasonable to be confident in the simulation predictions of the properties of ethane at even higher pressures where measurements are scarce (the data in reference 8 do not go beyond 70 MPa). Figure 2b shows the predicted isobar at 150 MPa. The data can be expected to be accurate to $\leq 2\%$.

2.2 *Discussion*

The data presented in this section show that it is possible to accurately predict the fluid phase properties of a molecular system using an effective 2-body potential fitted to an absolute minimum of experimental data. Similar results have been obtained for chlorine (9), methanol (10), heavy hydrocarbons (11) and mixtures such as water/methanol (12). It appears that, at least for fluid phases, the details of the molecular interactions are not required for accurate predictions of densities and

Table 3 Supercritical densities for ethane from NPT simulation. Experimental results for ethane at 150 MPA are not available (NA)

T (*K*)	*Pressure* *MPa*	*Predicted density* *mol/dm^3*	*Experimental density (8)* *mol/dm^3*
300	70	16.52	16.56
460	70	12.52	12.68
600	70	10.00	10.13
300	150	18.39	NA
460	150	15.51	NA
600	150	13.28	NA

pressures. Further, although 3-body forces are undoubtedly significant even in simple fluids, they can be subsumed within 2-body effective potentials if errors of a few percent or less in physical properties are acceptable.

3 ORGANIC INTERFACES AND ATOMIC FORCE MICROSCOPY

Organic interfaces are of immense scientific and technological interest. There exist a wide range of structures from Langmuir-Blodgett films (ordered multilayers constructed by repeated dipping of an inorganic support through a monolayer of organic molecules at a water interface) to the lipid bilayers forming cell walls. One characteristic of such organic interfaces is that they are non-rigid *i.e.*, they are easily perturbated by external probes or environmental changes (such as pH). It is of interest to consider to what extent they can be analysed using invasive techniques such as Atomic Force Microscopy (13) and if the interface is modified by the experiment. Molecular dynamics simulation is able to provide valuable insights into the nature of the interaction between the instrument and the interface.

3.1 Atomic Force Microscopy of Organic Interfaces

The Atomic Force Microscope (AFM) measures interactions (electrostatic, van der Waals, steric,...) between a scanning tip and a surface on a nanometre scale (see Figure 3).

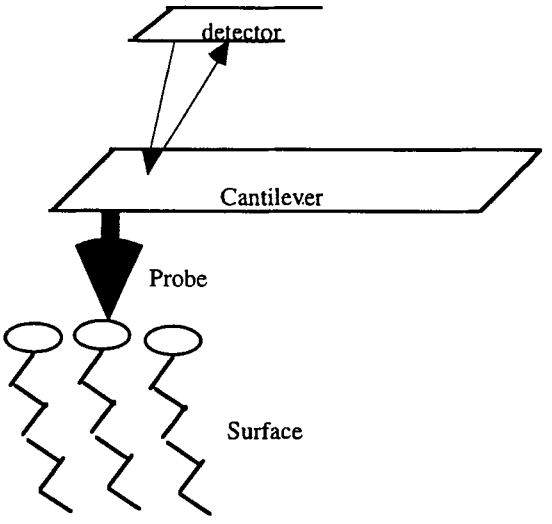

Figure 3 Schematic representation of an Atomic Force Microscope (AFM). The AFM image is a map of the force registered by the probe at each point in the plane of the surface as the sample is scanned. The deflection in the cantilever attached to the probe is detected optically and the force calculated from its spring constant. Forces exerted on the probe for the systems considered here were between 0.1 and 60 nN.

AFM scans can be performed either in a constant height mode where the sample is kept at a constant height and the varying force on the probe as it scans over surface features is registered as a deflection in the cantilever or in constant force mode where the deflection of the cantilever is kept constant. Constant force mode produces the least disruptive force and allows accurate height information to be obtained.

Experiments were carried out (at constant force) using a digital instrument nanoscope (III) AFM on the surface of cadmium behenate (C_{22}) Langmuir-Blodgett trilayer films supported on mica (14). Figure 4 shows the AFM image obtained for a mica surface over 10 nm. The surface is ordered on the atomic scale. Figure 5 is a low resolution image of the surface of a trilayer. It shows a trough excavated by applying a strong force to the probe and then scanning at a lower non-disruptive force. Finally Figure 6 shows the trilayer surface at high resolution. The molecular structure (quite different to that of the mica support) can be seen over a ten nanometre section. A hexagonal lattice is apparent containing distorted regions. The molecular area is $\sim 24 \pm 4\,\text{Å}^2$.

Figure 6 clearly demonstrates that it is possible to obtain atomic resolution images of 'soft' organic interfaces (see also reference 16). However, Figure 5 also suggests that changing the applied force can also cause considerable damage. The local pressures imposed by the probe even with 'non-disruptive' forces are immense $\sim$ 1nN applied over $\sim 1\text{nm}^2$ give pressures of GPa's. It is therefore at least possible that the surface structures observed during high resolution AFM experiments represent not the native surface but high pressure perturbations. This question is explored in the next section using molecular dynamics simulation.

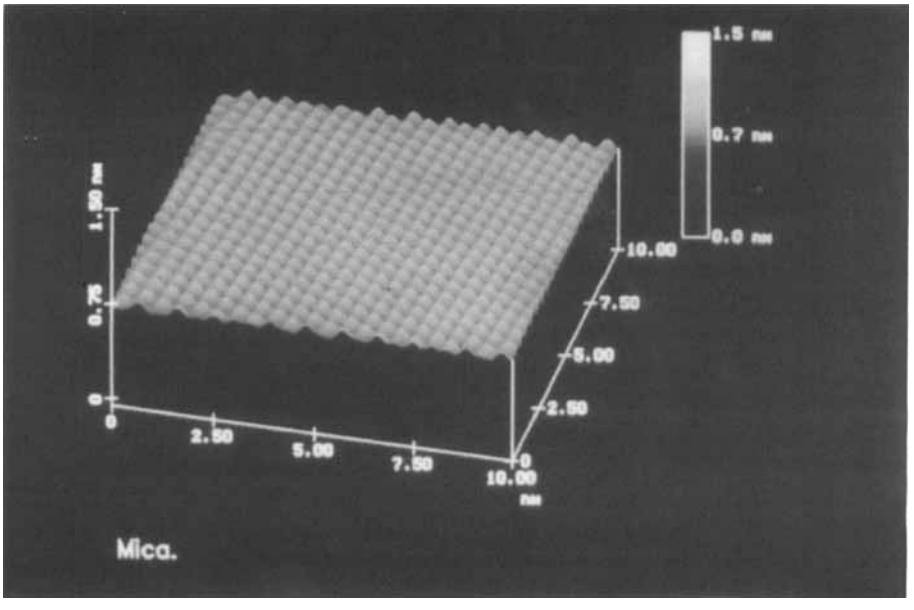

Figure 4 AFM image of a cleaved mica surface. See color plate I.

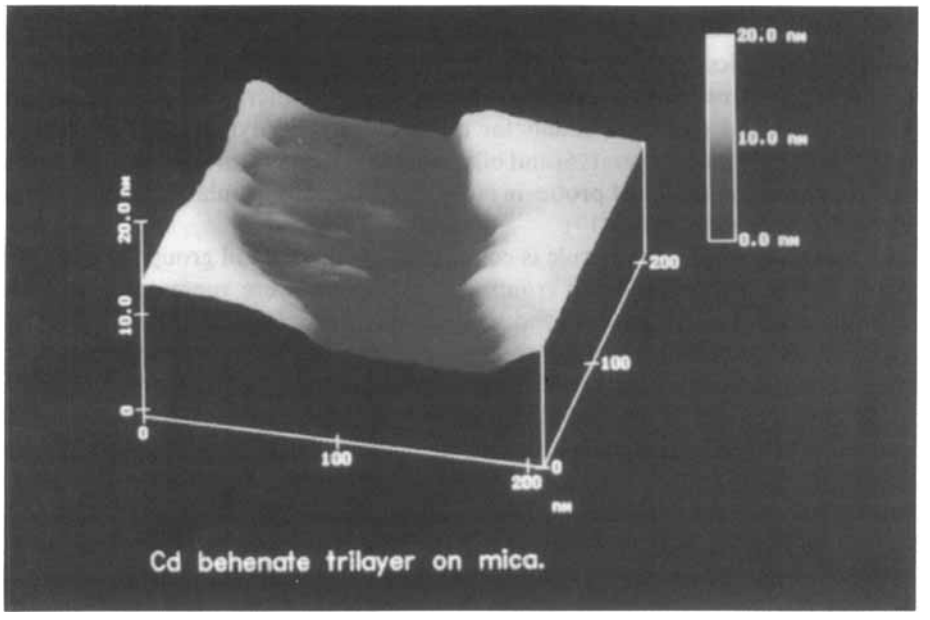

Figure 5 AFM low resolution image of a trough created in the surface of a cadmium behenate (C_{22}) trilayer Langmuir-Blodgett film supported on mica. See color plate II.

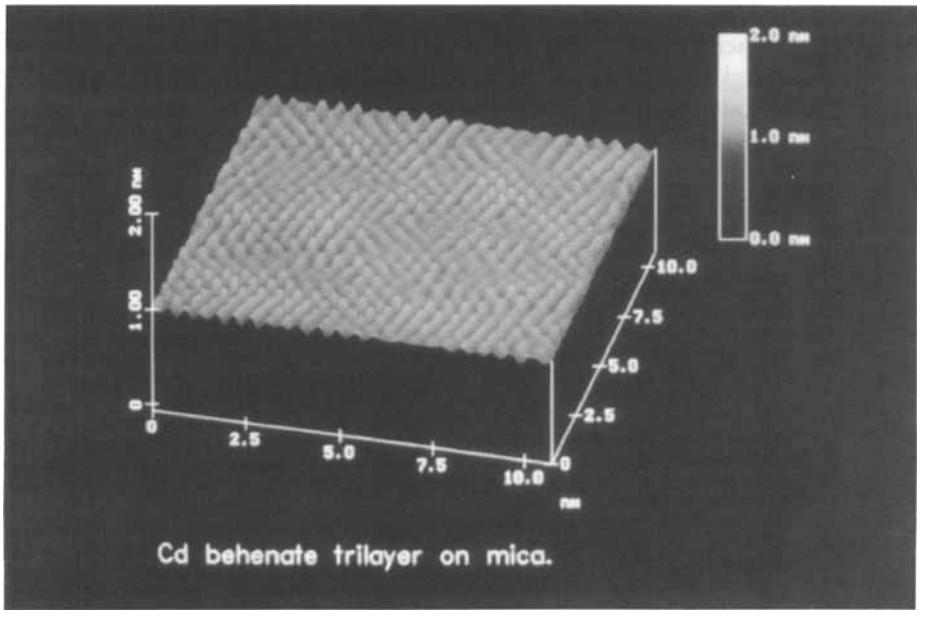

Figure 6 AFM high resolution image of the surface of a cadmium behenate (C_{22}) trilayer Langmuir-Blodgett film supported on mica. See color plate III.

3.2 *Molecular Dynamics Simulation of Atomic Force Microscopy*

Molecular dynamics simulation is able to provide valuable insights into the nature of the interaction between the instrument probe and the interface. We have recently reported molecular dynamics results for the structure and dynamics of equilibrated model stearic acid monolayers (15) and bilayers (16) at temperatures upto 298 K. In this section the use of model AFM probes in molecular dynamics simulation to characterise surface structure is discussed (17).

The model stearic acid molecule is composed of a methyl tail group, 16 methylene groups, and a carboxylic head group. All hydrogens were represented explicitly except those on the tail group. Bond lengths were fixed; however, bond angles and rotationed about carbon-carbon bonds were controlled by harmonic and dihedral potentials respectively. The dipole moment of the head group was represented by partial charges placed on the four atoms of the head group giving an overall molecular dipole of 1.79 D. Each atom and partial charge in the molecule interacted with all other molecules within a cut off. They also interact with a structureless surface via a LJ 9–3 potential and image charges. In summary, the model organic interface was composed of fully flexible chain molecules with explicit dispersion and electrostatic interactions. The functional forms and parameters for the force field employed are described in detail in references 15–17.

As the size and shape of the area of the AFM probe which is responsible for producing the image are not known with any certainty, two models of the AFM were employed (see Fig. 7). A sharp rigid tip in the form of a triagonal pyramid formed of 394 carbon atoms in a diamond lattice and a flat featureless surface with one protruding carbon atom. The embedded atom senses the local forces due to the surface molecules.

A model interface was created by placing an 8 by 8 hexagonally close packed (with 20.6 $Å^2$ $molecule^{-1}$) monolayer of stearic acid molecules on a structureless hydrophilic surface with periodic boundary conditions in the plane of the surface. The molecules were placed head down on the surface and the system simulated for 110 ps (75,000 steps).

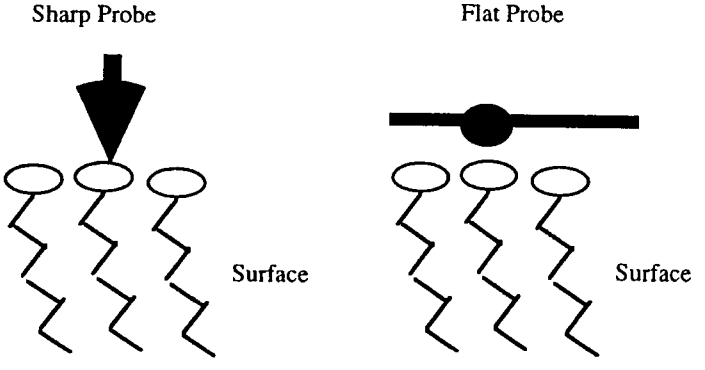

Figure 7 Two model probes employed to scan the surface of stearic acid films using molecular dynamics.

During a high resolution AFM experiment an area of (say)3*3 nM^2 will be scanned with a frequency of ~50 Hz. In the molecular dynamics simulation a time step of 2 fs was employed, hence such a scan would take 10^{13} molecular dynamics steps. On the time scale of the simulations the probe does not move, scanning by the model probes is performed by averaging the forces on the static probe at a series of positions over the surface. At each scanning position the probe was lowered into the film in a series of small steps, the stearic acid molecules being allowed to re-equilibrate around the probe at each step (17).

Figure 8 shows a force map of the stearic acid monolayer surface constructed from a series of molecular dynamics runs employing the sharp probe at a mean probe force of 0.6 nN, which is close to typical forces used experimentally. The map shows hexagonal ordering as expected; however, the maxima and minima along the x-direction correspond not to the mean positions of tail groups and the gaps between them but the reverse. The most repulsive forces occur when the probes are between the tail groups. Detailed analysis (17) of the results shows that when the probe is directly above a tail group the molecule below it can collapse by changing its conformation and the probe experiences a weaker force than expected. Consequently the force map is inverted. As the temperature is lowered the molecules become less flexible and by 75 K molecules can no longer collapse. As a consequence the force map reverts to show maximum forces above tail groups.

Figure 9 shows the force map of the same surface using the planar tip. Again the map displays hexagonal ordering but now the peaks in the surface force correspond to tail group positions. The planar probe geometry minimises the disruption of the film. The higher overall surface force is a consequence of the increased interaction with the planar surface to which the probe atom is attached. The variation in probe repulsion over the surface is of the same magnitude as that for the sharp probe.

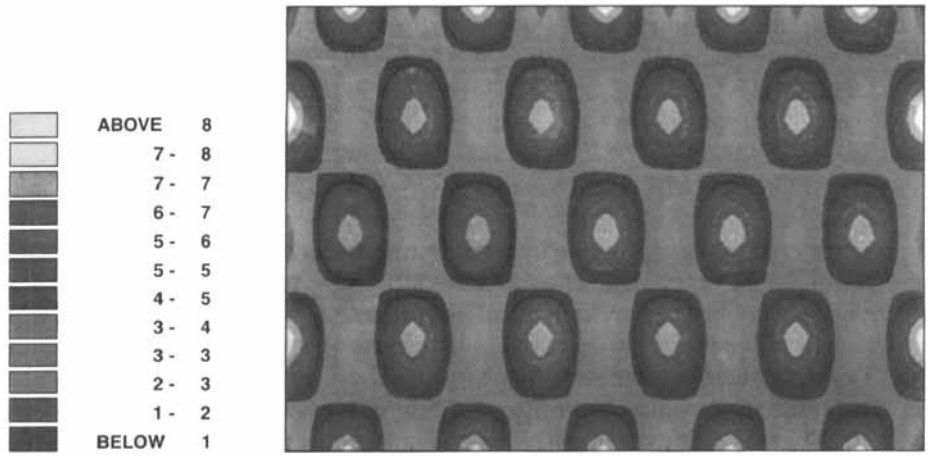

Figure 8 Contour plot of the average force exerted on a sharp AFM probe by a stearic acid surface, head group area = 20.6 $Å^2$ molecule $^{-1}$, T = 298 K. A scale point 3 corresponds to a force of 0.42 nN, scale point 9 to 0.95 nN (17). See color plate 1V.

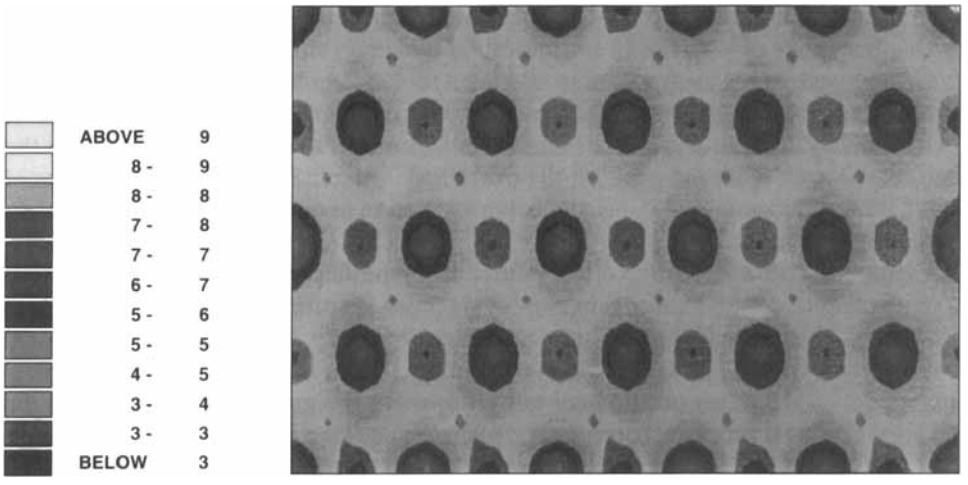

Figure 9 Contour plot of the average force exerted on a planar AFM probe by a stearic acid surface, head group area = 20.6 Å^2 molecule^{-1}. $T = 298$ K. A scale point 3 corresponds to a force of 6.66 nN, scale point 9 to 6.84 nN (17). See color plate V.

3.3 *Discussion*

Molecular dynamics simulation of the AFM experiment with organic films shows that it is possible to obtain reasonable force maps with the probe considered as a static object. However, the image obtained depends on the geometry of the model probe. A sharp probe produces the collapse of surface molecules and an inverted image with the greatest force registered when the probe is between molecules. The planar probe produces a truer image with the large flat surface stabilising the solid structure of the organic film. However, if the planar probe is lowered too far into the surface, the surface structure is likely to first be enhanced over the native film and then destroyed. These results illustrate the importance of simulating the system of interest in order to better understand the experiment. It is clear that AFM may modify the surface structure of organic films.

4 TRANSPORT IN MICROPORES

The properties of molecules in microporous matrices (pore widths/diameters < 20 Å) are of both fundamental (influence of external fields, quasi 1 and 2-dimensional behaviour) and applied (separations, catalysis) interest. Recently a large body of work has appeared in the literature describing simulations of equilibrium phase behaviour and diffusion in micropores (*e.g.* 18–21). Most real adsorption and catalytic processes however operate under non-equilibrium conditions. Moreover the physics of molecular transport along gradients in micropores is unclear. In this section the problem of non-equilibrium mass transport in micropores is investigated using molecular simulation methods. In particular results recently obtained by Cracknell *et al.*, (22) using novel combined Monte Carlo/molecular dynamics methods will be described.

Under isothermal conditions the gradient of the chemical potential is the driving force for mass transport. Such transport can be considered to have both a diffusive and a (co-operative) viscous component. Equilibrium molecular dynamics can be used to calculate self-diffusion coefficients D_0. From the mean square displacement of the molecules using the Einstein relation (or from the velocity autocorrelation function). Assuming the Darken equation (23), then the flux through a pore with density gradient $d\rho/dz$ is

$$J = (D_0 d \ln P/d \ln \rho)\, d\rho/dz$$

where $d \ln P/d \ln$ is the gradient of the equilibrium isotherm. This expression assumes Ficks law (the linear relationship between flux and density gradient) and D_0 remains valid arbitarily far from equilibrium. Possible viscous effects are not included. Furthermore it is by no means clear that the density gradient inside a micropore should always be linear.

Recently Cracknell *et al.*, (22) developed a new method which can simulate the mass transport along a chemical potential gradient directly. It therefore includes all possible viscous and diffusive components of the flux and can be used far from equilibrium. The method employs grand canonical molecular dynamics to maintain the ends of a micropore at different chemical potentials and a standard molecular dynamics algorithm to move the particles between the ends under the influence of the chemical potential gradient. The next section briefly describes the GCMD method. The subsequent section describes the NEMD method of Cracknell *et al.* and some of their results.

4.1 *Grand Canonical Molecular Dynamics*

The feasibility of grand canonical molecular dynamics GCMD was first demonstrated by Cielinski and Quirke in 1985(24). They tested an *ad hoc* GCMD method for the properties of bulk LJ's fluids. The chemical potential of a molecular dynamics simulation was controlled by superimposing the particle insertion and deletion step from grand canonical Monte Carlo simulation. As long as the number of creations and deletions was small, properties such as diffusion coefficients were accurately predicted. In their work a trial insertion and deletion was attempted every time a molecule crossed the periodic boundaries. The velocities of the inserted molecules were chosen from a Maxwell-Boltzmann distribution and the overall temperature maintained by temperature scaling. Table 4 shows a comparison at several state points of the predicted thermodynamic and transport (diffusion) properties obtained by GCMD and

Table 4 Comparison of grand canonical molecular dynamics with conventional methods. † from reference 25, ‡ obtained by Widom insertion, ° from molecular dynamics at the same state point. units of $(m^2/s)/10^{-10}$ Results from reference 24.

Type	T^*	μ^*,ex	ρ^*	$-U^*$	P^*	D
GCMC	4.00	1.01	0.23	1.24	1.06	°4.95
GCMD	4.00	1.00	0.23	1.22	1.04	4.96
GCMC†	2.00	0.85	0.64	4.02	2.12	°4.98
GCMD	2.00	0.84	0.64	4.01	2.20	4.95
MD	0.71	−4.99‡	0.80	5.82	−0.54	8.78
GCMD	0.70	−4.98	0.79	5.88	−0.67	8.72

conventional simulation (GCMC and MD). There is good agreement. Later workers have developed other GCMD methods (26, 27).

For applications such as that discussed below where the GCMD acts as a gateway to a particle bath for an adjacent conventional molecular dynamics simulation and the dynamics of the molecules in the GCMD is not of primary concern; the restrictions on the fraction of particle insertions and deletions can be relaxed.

4.2 *Direct Prediction of Particle Flux in Micropores*

Cracknell *et al.* (22) applied the GCMD scheme to the two ends of a micropore, creating source (high chemical potential) and sink (low chemical potential) regions containing Lennard-Jones atoms. Atoms leaving the ends of the pores were destroyed, atoms inserted by the GCMD algorithm were given a streaming velocity calculated from the average of the previous 1000 steps. Atoms leaving the end regions and entering the pore were moved using conventional molecular dynamics except that temperature rescaling was carried out on the velocities normal to the flow direction. The temperature along the direction of flow was equilibrated by molecular collisions.

In spite of very high pressure differences between source and sink regions (~ 35 atm in 50 Å) the density gradient was found to be, to a good approximation, linear. The flux was also found to vary (approximately) linearly with the gradient, confirming that Ficks law is obeyed far from equilibrium. Figure 10 shows the fluxes (J^*) obtained in reduced units.

If the transport diffusivities (the gradients of the curves) are compared to the best estimate from equilibrium molecular dynamics of the same system (same average density) *i.e.*, $D_0\ d\ln P/d\ln\rho$, the nonequilibrium diffusitivies are found to be between 2 and 4 times greater (22). This is indicative of a substantial viscous contribution to mass transport in micropores.

The new NEMD method will allow the elucidation of transport processes far from equilibrium. It can easily be extended to different pore types and to mixtures. Given the complexity of the equilibrium phase behaviour of simple molecules in pores (19) it can be expected that the transport behaviour is equally, if not more, diverse.

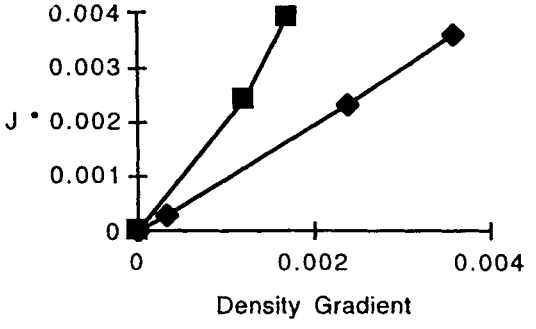

Figure 10 Methane flux in a graphitic micropore of width 9.525Å^2 at 296.2 K (adapted from reference (22)). The units are flux, $J\sigma^3\ (m/\varepsilon)^{1/2}$ and gradient $d\rho/dx\,\sigma^4$. The upper curve corresponds to higher average pore densities than the lower curve.

Acknowledgements

I would like to thank my colleagues D. J. Tildesley of Southampton University, and R. Cracknell and D. Nicholson of Imperial College, University of London for useful discussions on a number of points raised in this paper. Figures 10 and 11 were reproduced with permission from reference 17, copyright American Chemical Society.

Reference

[1] D. Fincham, N. Quirke and D. J. Tildesley, "Computer simulation of molecular liquid mixtures 1. A diatomic Lennard-Jones model mixture for $CO_2/C_2H_6$6" *J. Chem. Phys.*, **84**, 4535 (1986).
[2] A. Z. Panagiotopoulos "Direct determination of phase coexistence properties of fluids by simulation in a New Ensemble", *Molecular Physics*, **61**, 813 (1987).
[3] A. Z. Panagiotopoulos, N. Quirke, M. Stapleton and D. J. Tildesley, "Phase equilibria by simulation in the Gibbs ensemble: Alternative derivation, generalisation and application to mixture and membrane equilibria", *Molecular Physics*, **63**, 527 (1988).
[4] W. L. Jorgenson, J. D. Madura and C. J. Swenson "Optimized intermolecular potential functions for liquid hydrocarbons", *J. Am. Chem. Soc.*, **106**, 6638 (1984).
[5] M. Wojcik, K. E. Gubbins and J. G. Powles, "The thermodynamics of symmetric two centre Lennard-Jones liquids", *Molecular Physics*, **45**, 1209 (1982).
[6] J. Fishcer, R. Lustig, H. Brietenfelder-Manske and W. Lemming, "Orthobaric properties of model fluids" *Molecular Physics*, **47**, 485 (1984).
[7] M. P. Allen and D. J. Tildesley, "Computer simulation of liquids", Oxford University Press, (1986).
[8] B. A. Younglove and J. F. Ely, "Thermophysical properties of fluids 11. Methane, ethane, propane, isobutane and normal butane", *J. Phys. Ref. Data*, **16**, 642 (1987).
[9] G. Galassi and D. J. Tildesley, "Phase diagrams of diatomic molecules using the Gibbs ensemble Monte Carlo method", *Molecular Simulation*, **13**, 11 (1994).
[10] M. E. van Leeuwen and B. Smit, "Molecular simulation of the vapor-liquid coexistence curve of methanol", *J. Phys. Chem.* (accepted).
[11] J. I. Siepmann, S. Karaborni and B. Smit, "Simulating the critical behaviour of complex fluids", *Nature*, **365**, 330 (1993).
[12] H. J. Strauch and P. T. Cummings,"Computer simulation of vapor-liquid equilibrium in mixed solvent electrolyte solutions", *Fluid Phase Equilibria*, **83**, 213 (1993).
[13] J. Frommer, "The emerging presence of scanning tunneling microscopy (STM) and atomic force microscopy (AFM) in organic chemistry", *J. Angew, Chem. Int. Ed. Engl.*, **31**, 1298 (1992).
[14] M. Callaway, D. J. Tildesley, S. Rodgers, J. Clint and N. Quirke (unpublished, 1992).
[15] K. S. Kim, M. A. Moller, D. J. Tildesley and N. Quirke, "Molecular dynamics simulations of Langmuir-Blodgett monolayers with explicit head-group interactions", *Molecular Simulation*, **13**, 77 (1994).
[16] K. S. Kim, D. J. Tildesley and N. Quirke, "Molecular dynamics of Langmuir-Blodgett films 11. Bilayers", *Molecular Simulation*, **13**, 101 (1994).
[17] M. Callaway, D. J. Tildesley and N. Quirke, "Reordering of surface phases during atomic force microscopy: A simulation study", *Langmuir*, **10**, 3350 (1994).
[18] R. F. Cracknell, D. Nicholson and N. Quirke, "A grand canonical Monte Carlo study of Lennard-Jones mixtures in slit pores 2: Mixtures of two centre ethane with methane", *Molecular Simulation*, **13**, 161 (1994).
[19] C. Lastoskie, K. E. Gubbins and N. Quirke, "Pore size heterogeneity and the carbon slit model: A density functional theory model", *Langmuir*, **9**, 2693 (1993).
[20] J. M. D. MacElroy and S. U. Suh, "Simulation studies of a Lennard-Jones liquid in micropores", *Molecular Simulation*, **2**, 313 (1989).
[21] J. Magda, M. Tirrell and H. T. Davis, "Molecular dynamics of narrow liquid filled pores", *J. Chem. Phys.*, **83**, 1888 (1985).
[22] R. F. Cracknell, D. Nicholson and N. Quirke, "Direct molecular dynamics simulation of flow down a chemical potential gradient in a slit-shaped micropore", *Phys. Rev. Lett.*, **74**, 2463 (1995).
[23] J. Karger and D. M. Ruthven, *Diffusion in zeolites and other microporous solids*, Wiley, New York (1992).
[24] M. M. Cielinski, *M. S. Thesis*, Uni. of Maine, Orono (1985); M. M. Cielinski, N. Quirke (unpublished 1985).

[25] D. J. Adams, "Grand canonical ensemble Monte Carlo for a Lennard-Jones fluid", *Mol. Phys.*, **29**, 307 (1975).
[26] T. Cagin and B. M. Pettit, "Grand molecular dynamics: A method for open systems", *Molecular Simulation*, **6**, 5 (1991).
[27] G. S. Heffelfinger and F, van Swol, "Diffusion in Lennard-Jones fluids using dual control volume grand canonical molecular dynamics simulation (DCV-GCMD)", *J. Chem. Phys.*, **100**, 7548 (1994).
[28] R. J. Sadus and J. M. Prausnitz, "Three body interactions in fluids: Molecular simulation of the vapor liquid phase coexistence of argon", (Preprint 1994).